It can be seen that the theory leads one to expect fewer neutrons than were observed; it predicts too few events of $n=2$ by one order of magnitude and too few events of $n=3$ by at least two orders of magnitude (except for Al). It should be noted that the data indicate that the probability of having $\nu \geq 3$, or $\mathcal{E} \gtrsim 22$ Mev, is about $\frac{1}{4}$ to $\frac{1}{3}$ for Pb, Bi, and Sn, while according to the calculations of Tiomno and Wheeler, and Rosenbluth, $P(\mathcal{E})=0$ for $\mathcal{E}>23$ Mev, and the probability of events with $\nu \geq 3$ is negligible.

The theoretical maximum excitation energy $\mathcal{E}=23$ Mev, which is inconsistent with the experimental results, comes from the assumption that the nucleons in the nucleus constitute a Fermi gas with a maximum energy of 20 Mev and from neglect of the interactions between nucleons. These interactions permit the momentum and energy to be distributed to more than one nucleon in the capture process and thus give rise to higher nuclear excitations.

The author wishes to thank the Ithaca Gun Company for the use of its tunnel. It is a pleasure to thank Professor Kenneth Greisen, Professor Giuseppe Cocconi, and Professor Philip Morrison, and Dr. Vanna Cocconi Tongiorgi for many helpful discussions.

PHYSICAL REVIEW VOLUME 90, NUMBER 5 JUNE 1, 1953

Proton-Proton Scattering from 1.8 Mev to 4.2 Mev*

H. R. WORTHINGTON, J. N. MCGRUER,† AND D. E. FINDLEY‡
University of Wisconsin, Madison, Wisconsin
(Received December 15, 1952)

Measurements of the scattering of protons by protons have been made at six energies in the range from 1.8 Mev to 4.2 Mev. At each energy, the differential cross section was measured as a function of angle from 6° in the laboratory system up to 45° or higher. In the angular range above 20°, the cross sections are determined to within ±0.3 percent. Below 20°, the uncertainties become larger, approaching ±0.6 percent at 6°. Departures from pure S-wave scattering are observed at all energies .These deviations are larger than can be explained by the experimental uncertainties. They closely resemble the effect of a negative P-wave phase shift of approximately −0.1° at 4 Mev and exhibit a reasonable energy dependence.

I. INTRODUCTION

A NUMBER of excellent surveys of experimental results on proton-proton scattering and their theoretical interpretation have appeared in the past few years.[1,2] It is generally concluded that the presence of higher phase shifts has not been established, and the need for improved accuracy in experimental data is strongly indicated.

In the present experiment the scattering of protons by protons is re-examined in the energy range from 1.8 Mev to 4.2 Mev with fractional percent accuracy. Information about the form of the interaction potential is sought through a more accurate determination of the S-wave phase shifts. By a closer inspection of angular distribution and by extending angular distribution measurements to smaller angles, the effects of higher angular momenta are sought.

II. GENERAL FEATURES OF SCATTERING CHAMBER

Details of the chamber design are shown in Figs. 1 and 2. The beam enters the chamber from the large collimating tube at the right, it traverses the chamber and is collected by a Faraday cup at the rear. Hydrogen gas at a pressure of 8-mm Hg fills the entire cylindrical chamber and provides the target. Scattering occurs everywhere along the path of the beam, but only that from a small region at the center of the chamber can reach the detector through the narrow slits of the analyzer. Details of the analyzer slit system can be seen in Fig. 3. The defining slits are mounted on dovetail slides in such a way that any one of three slit sizes may be selected by varying the vertical positions of the slides. Manipulating rods in the top cover of the chamber enable the slits to be changed without interruption of operation.

The analyzer and detector are mounted on a large angle-wheel which can be rotated to any position within ±100° of the forward direction. This wheel is rim supported and rim driven. It was originally the meridian circle of an astronomical telescope and has near its rim an angle scale 50 cm in diameter graduated at 2-minute intervals of arc. On division marks, angles can be set within about 0.001°. As index marks, two fine quartz fibers are used, one in each of the two backward 45° positions. They are mounted on open frames close above the scale and are viewed by telescopes mounted in the lid.

A proportional counter with a thin nickel window

* Supported by the U. S. Atomic Energy Commission and the Wisconsin Alumni Research Foundation.
† Now at University of Pittsburgh, Pittsburgh, Pennsylvania.
‡ Now at North American Aviation, Inc., Downey, California.
1 Yovits, Smith, Hull, Bengsten, and Breit, Phys. Rev. **85**, 540 (1952).
2 J. D. Jackson and J. M. Blatt, Revs. Modern Phys. **22**, 77 (1950).

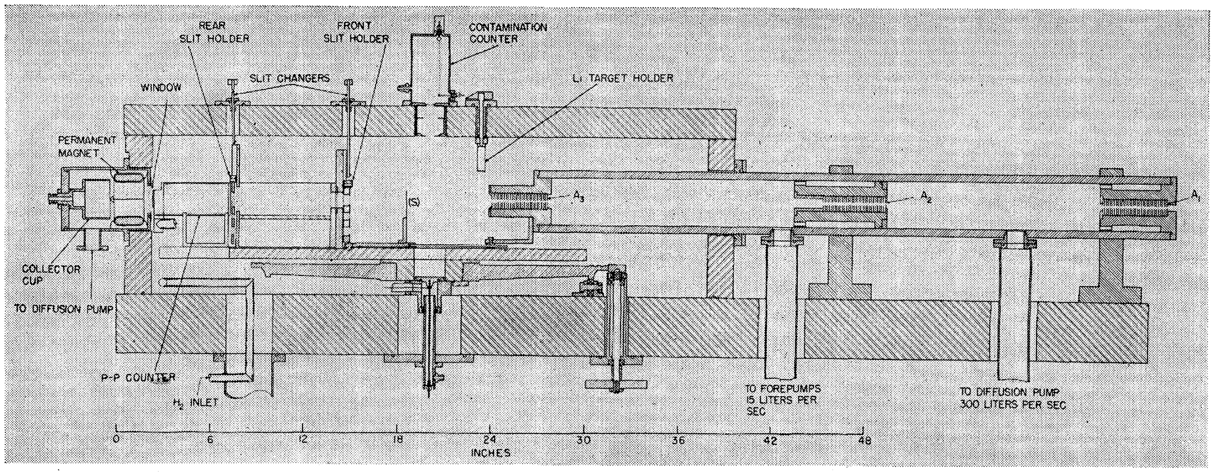

FIG. 1. Vertical cross section of chamber with analyzer slit assembly at zero-angle.

serves to detect scattered protons. The counter gas may be either argon or hydrogen at pressures up to one atmosphere. The gas connection for the counter is provided by the same line that serves as a high voltage coax and as a low capacitance signal lead. This conduit is equipped with a vacuum-tight rotary joint on the axis of the wheel. Electrical continuity is maintained in this rotary joint by means of a thin torsion wire.

Details of the collimator tube are seen in Fig. 1. The defining apertures, A_1 and A_3, are 1.5 mm in diameter and are spaced 1 meter apart. Aperture A_2 is 2 mm in diameter and serves as a baffle to shield the diaphragms behind it from the beam. These diaphragms and those behind apertures A_1 and A_3 are not a part of the collimating system proper and are not exposed to the beam. They form a series of capillary constrictions for the differential pumping system. A hydrogen flow of 18 atmospheric liters per hour maintains a pressure of 8-mm Hg in the chamber. Pressures in successive stages of the flow system are then 0.2-mm Hg, 2×10^{-4} mm Hg, and high vacuum. With this system no foil window is needed and no appreciable amount of gas is present between the defining apertures of the collimator. Thus, the uncertainty as to the energy loss at the entrance of the chamber is made negligible and the spreading of the beam by scattering is so slight that the beam may be collimated to ±6 minutes without appreciable loss of intensity.

The collector cup is recessed in the rear wall so that the analyzer assembly may be rotated freely through zero. A 1/20-mil nickel window isolates the evacuated region around the collector cup from the chamber. This window is 1.67 inches in diameter to insure a high efficiency in beam collection despite the spreading of the incident beam in the gas of the chamber. Suppression of secondary electrons from the window foil

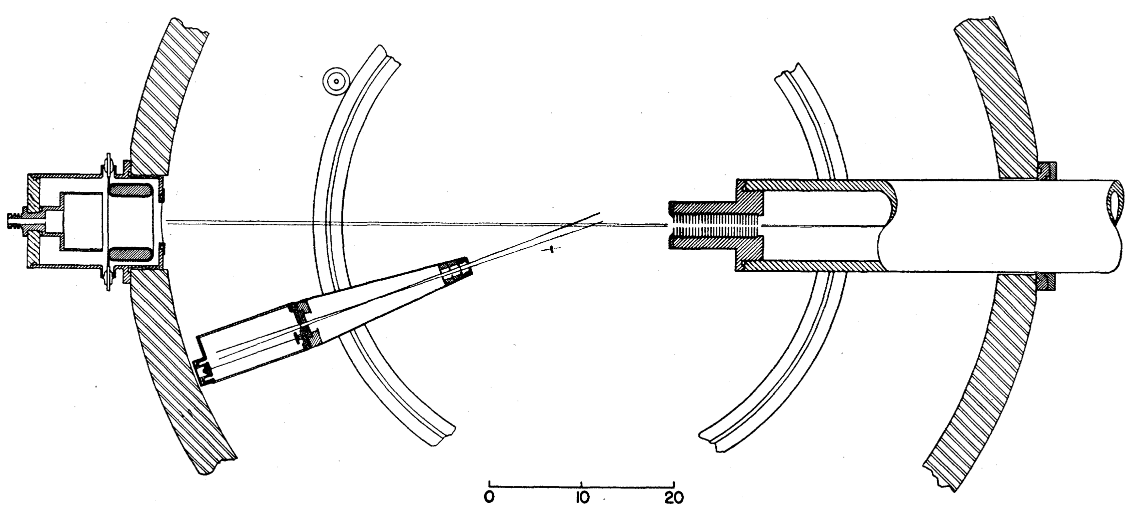

FIG. 2. Scale diagram showing cross section of principal components in the plane of scattering.

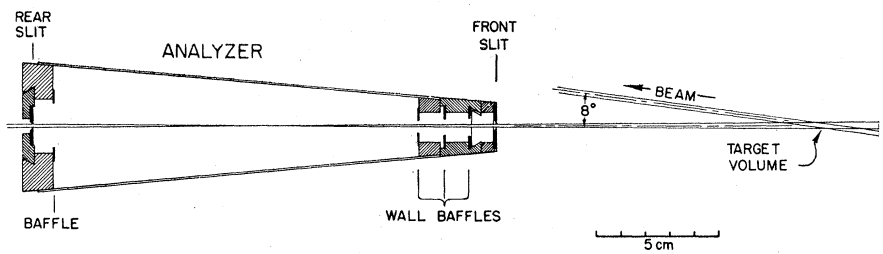

FIG. 3. Scale diagram of analyzer slit system. The dovetail slides at front and rear carry three sets of slits: a 1-mm set (shown), a 2-mm set, and a 4-mm set.

and from the cup is accomplished by means of both magnetic and electrostatic fields.

In the lid of the chamber is a fixed counter which serves to monitor the purity of the gas. Protons scattered from hydrogen at 90° have zero energy, whereas those scattered from any other gas have appreciable energy. Thus, the 90° counter responds only to scattering from contaminant gases.

A movable shield (S) is shown in the drawings. This shield is so devised that it is always interposed between the exit orifice of the collimator and the entrance slit of the analyzer. It thus obstructs the most probable path by which protons could reach the counter without first having been scattered in the gas. This shield also serves to protect the counter from the direct beam as it passes through the zero angle.

III. SCATTERING GEOMETRY

G Factor

The yield of scattered protons is given by the expression

$$Y = Nn\sigma(\theta)G/\sin\theta, \quad (1)$$

where N is the number of incident protons, n is the number of target atoms per unit volume, and G is the so-called G factor of the analyzer slit system. In the notation of Fig. 4,

$$G = 2b_1A/R_0h, \quad (2)$$

where $A = 2b_2l$ is the area of the rear aperture. In the present experiment the quantity $\sigma(\theta)\csc\theta$ could vary by a factor of 600 in a single run. Three different G factors were therefore needed to maintain the counting rate within a factor of ten. The values were chosen so that a beam current of 0.25 microampere and a hydrogen pressure of 1-cm Hg would give counting rates between 100 and 1000 counts per second.

Detailed features of the geometry were chosen to maximize the angular resolution and minimize geometrical errors. The rear aperture was made in the form of a long narrow rectangle since angular resolution is less sensitive to slit height than slit width. In the region of low angles the error due to slit height is negative, while that due to slit width is positive. By a suitable choice of slit proportions these errors may be made to cancel. With $R_0 = 31.8$ cm and $h = 18.8$ cm, the optimum proportions were found to be $b_1 = b_2 = b$ and $(l/2b) = 5.1$. These relationships were obtained using a detailed expression for the geometrical errors in the yield given by Breit, Thaxton, and Eisenbud.[3] The Rutherford cross section and its derivatives were substituted into the error expression along with the approximation $\cos^2\theta = 1$, both of which are good approximations at small angles. The error expression was then set equal to zero to obtain the conditions for cancellation of errors. With the above proportions, the geometrical errors vanish independently of energy, angle, and slit size in the region of low angles, where such errors are significant. Identical proportions were used in each set of slits. The slit widths corresponding to the three G factors are $2b = 1$ mm, 2 mm, 4 mm. These widths are used hereafter to identify the three different slit systems. The half-angles of the systems are 18′, 36′, and 1°13′, respectively.

Angular Accuracy

The accuracy of low angle measurements depends most critically upon the accuracy of angle setting. With the angle scale previously described, angles could be set within about one-thousandth of a degree on the division marks. For alignment purposes, the same degree

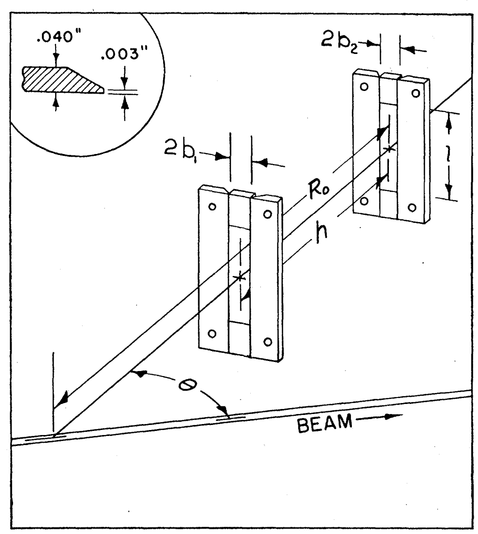

FIG. 4. G factor dimensions and method of construction of rectangular apertures. Slit jaws were ground by Gaertner Scientific Corporation. Edges were finished by a "liquid lapping" process. Side jaws are made of stellite and spacers of hardened stainless steel.

[3] Breit, Thaxton, and Eisenbud, Phys. Rev. 55, 1018 (1939).

of accuracy is not required. By making supposedly symmetrical readings to the left and to the right of the beam, one may eliminate the first-order alignment errors in the average. The second-order terms which remain are about two orders smaller in numerical magnitude; e.g., an asymmetry of ± 1 percent between the left-right readings corresponds to an error of about 0.1 percent in the average. A great advantage is thus obtained by using the average of "symmetrical" readings, and the ultimate accuracy is made to depend upon the accuracy with which the interval $2\theta_0$ is known rather than upon the accuracy of the zero alignment. In the presence of simultaneous misalignments of various kinds, the relationship between the asymmetry and the error in the average becomes less favorable. For this reason the specifications for alignment were based upon the requirement that the asymmetry introduced by any single error should not exceed $\pm\frac{1}{2}$ percent at 10°. The corresponding error in the average yield should then be negligible. In terms of angular alignment this amounted to a tolerance of $\pm 0.01°$. Corresponding linear tolerances were deduced for the various components of the system. In general, those tolerances were of the order of one-thousandth of an inch.

Method of Alignment

Alignment of the components of the chamber was accomplished by means of an optical projection system, making use of the fact that the images of colinear objects are also colinear. The analyzer was set at the zero angle of scattering, where all critical apertures should be centered on a common line passing through the axis of rotation. This axis was marked by means of a vertical fiber. A lens was set up in the approximate position of the collector cup so that it could project images of the apertures into the open space behind the chamber. Optical resolution was maintained for each image by removal of intervening apertures. All apertures were designed to be accurately replaceable. The series of images were checked for alignment by means of a cross-hair which was arranged to move in a straight line approximately parallel to the image line. At each position, the lateral distance between the image center and the cross-hair was measured by means of a traveling microscope. The displacements of the images from the line of motion of the cross-hair were then used to calculate the displacements of the objects from a corresponding straight line in the chamber.

Results of the final alignment are shown in Fig. 5, where slit positions are plotted with respect to the axis of the collimator on a lateral scale that is enlarged 200 times. The 1-mm slits are seen to be aligned within ten seconds of arc and within 1 mil. The 2-mm and 4-mm slits are less accurately aligned but are quite satisfactory. In the vertical plane the alignment was checked by the same method and was found to be correct within one mil.

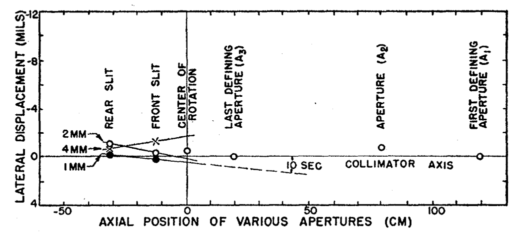

FIG. 5. Plot showing the alignment of the three analyzer slit systems relative to the incident beam. The lateral scale is expanded 200 times.

IV. COMPENSATION FOR MULTIPLE SCATTERING

The accuracy of scattering experiments using gas-filled chambers is dependent upon the existence of compensation processes whereby particles that are scattered out of a beam are replaced by particles scattered into it from surrounding regions. Such processes are inherent in the scattering geometry and are very effective. As much as 5 percent of the flux in the scattered beam may be exchanged before reaching the detector, whereas the introduction of an uncertainty of more than 0.03 percent by this effect was considered undesirable. A careful analysis of the compensation processes was necessary to determine the degree to which they are intrinsically effective and to establish criteria for the design of baffle systems. Formulas were obtained whereby the errors due to baffles were made negligible, and the errors inherent in the compensation process were shown to be so small that corrections were scarcely necessary in the range of energies and angles covered.

Figure 6 illustrates the principal mechanism of compensation, which involves an envelope of flux surrounding a central beam. A wedge-shaped beam from a line source is taken as an example. There is an envelope above and below the beam which extends the illumination beyond the edges of the slit, as indicated by shading. A pair of compensating scattering events are shown by the arrows. If the scattering conditions are completely symmetrical for this pair of events, the probability of compensation is unity. It can be shown by simple qualitative arguments that compensation is provided for any scattered particle which strikes the plane of the slit within the area illuminated by the envelope. A net loss results only from scattering which falls outside of this area. Thus, if the envelope is made sufficiently thick, only single-scattering events of relatively large angle will be important in the loss and the error may be computed quantitatively on that simple basis, using the Rutherford cross-section values. The fractional error due to the limited size of the envelope in Fig. 6 is given by the expression

$$\epsilon = \frac{\pi n}{6}\left(\frac{e^2}{E}\right)^2 \frac{L^3}{x_1^2 - x_0^2}. \tag{3}$$

The term $(e^2/E)^2$ comes from the Rutherford cross section for proton-proton scattering. For $E=1$ Mev and n corresponding to 1-cm Hg, the error is

$$\epsilon=0.6\times10^{-6}\frac{L^3}{x_1^2-x_0^2}(\text{cm}^{-1})\text{ percent.} \tag{4}$$

If the error is equal to a few tenths of a percent, the assumptions involved in the formula are valid. If the error is a few percent, the assumptions should be checked by referring to detailed expressions for the multiple scattering distribution.[4,5]

The above formula may be applied directly to the problem of multiple scattering in the vertical plane of the analyzer. In that plane, the scattered beam is defined by the rear aperture of length l at a distance R_0 from the incident beam. The top and bottom ends of the front slit serve as baffles and are spaced widely enough apart to permit a scattering envelope to exist above and below the beam. From the vertical extent of the illumination pattern on the plane of the rear slit one can calculate the error using Eq. (3). This formula also applies to scattering inside the analyzer in the horizontal plane (see Fig. 3). In that application each element of width of the front slit may be regarded as a source of flux; the wall baffles limit the size of the envelope and give rise to an intensity pattern on the plane of the rear slit similar to that shown by the shaded area in Fig. 6. From the width of that illumination pattern and the width of the rear slit, one can calculate the error.

It is clear that the flux required to form the envelopes inside of the analyzer must come from various parts of the main beam. Care must therefore be taken to see that shields and baffles outside of the analyzer do not conceal any part of the main beam that is required to supply flux for these envelopes.

The scattering envelope is not the only mechanism of compensation required in the system, but it is found that baffles and shields which are properly designed to meet the requirements for effective compensation by means of scattering envelopes will satisfy the requirements for compensation in other respects as well. The baffles in the present analyzer are so designed that their effects at 1 Mev and 1-cm Hg pressure are less than 0.2 percent.

The intrinsic effectiveness of the compensation for multiple scattering depends not upon the details of the geometry but upon the degree of symmetry which exists between the scattering events which cause loss of flux and those which provide compensation. At small angles, the variation of intensity with angle is so great that the compensation process becomes unbalanced and an error results. The error is found to depend mainly upon the second derivative of the cross section. It is important only at small angles and is positive in sign there. It depends also upon the mean-squared deviation of the gas-scattering distribution and derives its energy dependence and pressure dependence mainly from that quantity. The error is essentially independent of the slit width but does depend somewhat upon the relative lengths of the paths in various parts of the chamber. For example, the scattering which occurs in the path between the collimator and the target tends to offset the effect of the scattering which occurs between the target and the first slit. The final expression for the intrinsic error due to multiple scattering in the present experiment is

$$\epsilon=0.01\cot^2\theta(PE^{-2})\text{ percent,} \tag{5}$$

where P is the pressure in cm Hg and E is the energy in Mev. This expression is based upon the Rutherford cross section and is applicable only at small angles. The error was evaluated for $E=2$ Mev and $P=1$-cm Hg according to the multiple-scattering distributions of Williams.[4] The dependence (PE^{-2}) is introduced as a convenient approximation. The largest error according to this formula occurred at 7°, 1.855 Mev, and was +0.15 percent.

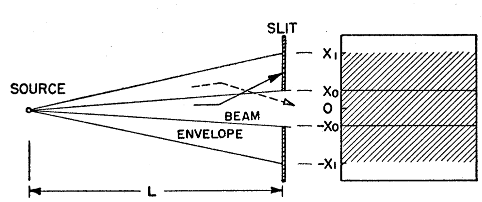

FIG. 6. Diagram illustrating the process of compensation for multiple scattering by means of a scattering envelope.

[4] E. J. Williams, Phys. Rev. **58**, 292 (1940).
[5] G. Molliere, Z. Naturforsch. **3a**, 78 (1948).

V. COUNTING EQUIPMENT AND PROCEDURES

The Counter

The proportional counter consisted of a cylinder of 2-in. i.d. and $2\frac{1}{2}$-in. effective length with a 3-mil molybdenum wire displaced 7/16 of an inch from the axis. It was large enough to accommodate the divergent flux from the largest analyzer aperture, which was about 20 mm×4 mm. Windows of two different thicknesses were used according to the scattering conditions, with a 1/20-mil nickel window for high pressure and high energy operation, and a 1/50-mil nickel window for low energy operation. The strength of the foils was utilized effectively by shaping the mounting surface so that the foil assumed the form of a segment of a cylinder $\frac{1}{2}$ of an inch in diameter. A 1/20-mil nickel foil of this form could withstand pressure differentials up to 25 psi across an opening 1 in.×0.28 in.

Pulse-Height Distribution

Counter performance was most favorable at moderate gas pressures, such that protons lost only a fraction of their energy. Ideally the pulse-height spectrum should consist of a narrow group of pulses completely separated from background noise, whereas, in actual practice, a spectrum such as that in Fig. 7 was obtained. A low

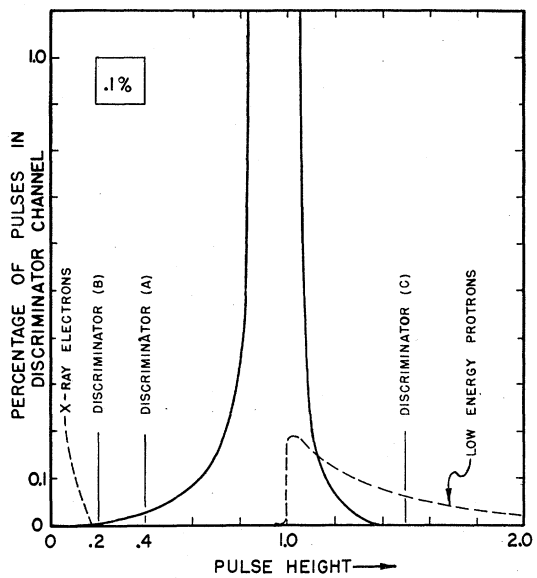

FIG. 7. Typical distribution of pulse heights. The spread in the main group of pulses (solid curve) is due mainly to scattering in the counter gas and in the counter window. The curve here represents the performance for 3-Mev protons with argon at 7-in. Hg in the counter and with a 0.00005 inch Ni window. The distributions of electrons and low energy protons are qualitative.

tail extends from the main group of pulses down to the x-ray noise.

During all yield measurements, two scalers were employed, one (*B*) with a discriminator set at 0.2 of the height of the main group and one (*A*) set at 0.4 of this value. The difference between the readings will be referred to hereafter as the (*B–A*) difference. This difference gives information in regard to the pulse spectrum and also provides a check upon scalar performance. During normal operation, its value was below 0.1 percent. Abnormally high values called attention to troubles. Only a minute percentage of the normal distribution falls below the level of discriminator (*B*) and is lost. Such low pulses appear to result from scattering in the counter window and in the counter gas and must be due in part to protons which scatter widely enough to strike the counter walls. At angles above 45°, the proton energies become quite low, and such scattering effects become appreciable. Analysis of a number of pulse-height curves, such as that in Fig. 7, showed a very good correlation between the percentage of degraded pulses in the (*B–A*) channel and the percentage in the extrapolated distribution below level (*B*). It was therefore possible to construct a correction curve in which the percentage correction for counter performance is given as a function of the percentage (*B–A*) difference. These corrections were insignificant below 45° and reached 0.7 percent only at the extreme angle of 60°.

X-Ray Background

A small background was observed in the (*B–A*) channel at low angles in every run. It was satisfactorily identified as being due to the superposition of electron pulses upon each other and upon the long exponential tails of the proton pulses. This correction was negligible above 12.5° and reached 0.2 percent at only seven data points.

Resolving Times

At high counting rates counts may be lost either because of the finite recovery time of the counting circuits or because of superposition of pulses. In the present work the pulse width was made the controlling factor. The "resolving time," which was approximately 3 microseconds, could then be determined at any time from information obtainable on the oscilloscope. The resolving time of the fast scalers (*A* and *B*) was made less than 1 microsecond for double pulses and less than 7 microseconds for triple pulses. Scales of 128 were used to maintain reasonable output counting rates. The mechanical registers could handle output rates up to 15 counts per second without introducing losses. The scaler for high pulses (*C*) was an ordinary scale of 64 operating at very low counting rates.

In calculating the counting loss resulting from superposition of proton pulses, one may safely assume that all of the pulses are of the same shape and height. It is easy then to determine the resolving time from the shape of the single pulses appearing on the oscilloscope. Resolving times were measured for each level of discrimination (*A* and *B*) using a calibrated oscilloscope sweep, and they are considered accurate to ± 10 percent. It may be noted that the resolution is not the same for the (*B*) and (*A*) discriminators and that consequently, the (*B–A*) difference must be corrected for counting loss. The counting loss at any level is given by the ratio of the resolving time at that level to the average time between pulses. With a steady beam the average time is calculated from the total running time and the total number of counts. The counting losses were generally less than 0.2 percent and rarely reached 0.4 percent.

VI. CORRECTIONS

Slit-Edge Scattering

The penetration of slit edges by protons results in a continuous distribution of low energy protons. Such protons were studied as high pulses in the present experiment. Figure 8 shows pulse size as a function of proton energy with argon at 7-in. Hg in the counter. By analysis of yield as a function of the setting of discriminator (*C*), the distribution of low energy protons can be determined.

For example, at a setting of 1.2 on the pulse-height scale of Fig. 8, discriminator (*C*) registers pulses from protons between 0.8 Mev and 2.7 Mev in energy. At a setting of 2.5, it will detect only those between 0.9 Mev and 1.3 Mev in energy. Such measurements do not give unambiguous information about the distribution of protons, however, because the energy interval changes at both its upper and lower limits and the variation in yield may be due to the change in either. This difficulty was overcome by repeating the measurements at several different counter pressures.

Not all of the high pulses are due to low energy protons; some are caused by superposition of regular proton pulses. The percentages of such pulses were calculated and deleted from each of the high pulse observations. In each case investigated, the distribution of low energy protons was found to be uniform over the observable energy range. The solid curve of Fig. 9 shows results obtained at 3.5 Mev with the 1-mm slits set at 8°.

Some high pulses are caused by the superposition of electron pulses upon those due to protons. These pulses are less than 1.2 in height and confuse the measurements below that level of discrimination. Thus, the protons in the upper 20 percent of the energy range could not be observed. The scattering by slit edges can be calculated theoretically, provided the energy lost in the process is small compared to the total energy.[6] The results of such a calculation for protons losing less than 20 percent of their energy are shown by the dashed lines in Fig. 9. Values are higher than one might expect from the experimental data but are not unreasonable, and they were accepted as the best available estimate for the upper 20 percent of the energy range. The combination of observed and calculated yields in Fig. 9

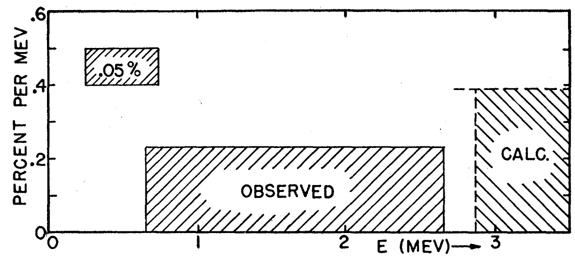

FIG. 9. Distribution of low energy protons from edges of 1-mm slits at 8°, 3.5 Mev. Such protons are observed as high pulses (see Fig. 8).

gives an error of 0.79 percent in the total yield at 3.5 Mev with the 1-mm slits set at 8°.

Measurements giving the percentage of protons scattered by slits were also taken at 1.855, 1.858, 3.527, 3.899, and 4.203 Mev with 1-mm slits. Corrections for other energies and the other slits were computed from these values using calculated relationships, and from these values the correction curves of Fig. 13 were constructed. An uncertainty of ±25 percent is assigned uniformly to all corrections for slit penetration. Within such limits the corrections are independent of the quantitative accuracy of the theoretical calculations.

Contributions of the various slits to the yield of slit-edge protons are best known from theoretical calculations. They show that the front slits contribute about two-thirds of the yield. The second important contribution to the yield of slit-edge protons comes from the rear slits of the analyzer, which contribute about one-third of the total. Another possible source of low energy protons is the last defining aperture of the collimator (A_3, Fig. 1). That aperture is strongly illuminated by the main beam, but it is followed by a narrow capillary which intercepts most of the scattered flux. The calculations show that the distribution of scattering from the steel edges of that aperture is so broad that less than 5 percent of the scattered flux emerges from the exit orifice. The net effect is negligible.

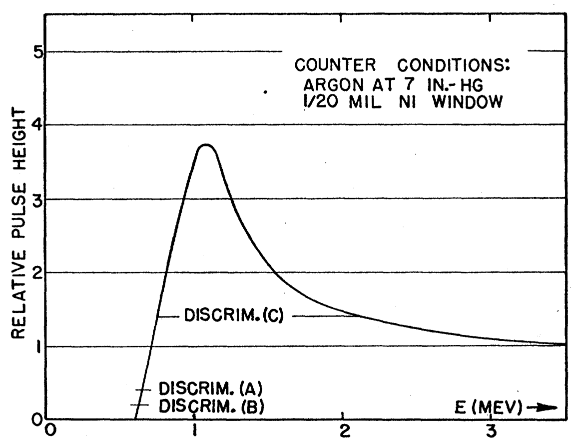

FIG. 8. A typical plot of pulse-height *vs* proton energy. Yield measurements are based upon the reading of discriminator (*B*). The channel between (*A*) and (*B*) is used to monitor counting conditions. Discriminator (*C*) is used to study the high pulses from low energy protons. Such curves are obtained by observing pulse height as a function of θ and applying the relation $E=E_0\cos^2\theta$.

[6] E. D. Courant, *Multiple Scattering Corrections for Collimating Slits* (Princeton University Press, Princeton, New Jersey, June 5, 1951). The formulas in this paper apply only for conditions such as those found at rear aperture of the analyzer where the acceptance angle for scattered flux is unrestricted. Approximate formulas for the other slits were obtained using information from B. Rossi and K. Greisen, Revs. Modern Phys. **13**, 267 (1941); and using the results of the analysis of compensation for multiple scattering.

Special Slit-Edge Correction at 3.9 Mev

The (*B–A*) differences at 6° and 7°, 3.9 Mev, gave (*B–A*) counting rates that were not consistent with the x-ray electron background. High pulse data at that energy also showed the presence of a strong group of pulses corresponding to protons of low energy. These pulses could conceivably have been the result of penetration of a baffle slit at some unsuspected thin spot, since the nominal limit for the baffles was only 4.3 Mev, with the stopping power of the counter window included. This explanation is unconfirmed, but, since the spurious yield was directly observed, a correction was applied. That correction is −0.38 percent at 6° and 7°. The uncertainty assigned to the correction is ±100 percent.

At 4.2 Mev, a similar effect was observed in the

(B–A) data at 6°, 7°, and 8°. The counting rates in excess of x-ray electron background were nearly three times as large as those observed at 3.9-Mev. A correction similar to that applied at 3.9-Mev is implied, but, in this case, the high pulse data did not include pertinent information. No correction was therefore attempted. Instead, large uncertainties were assigned to the 6°, 7°, and 8° points. Those uncertainties were sufficient to include the various possible values of error that had been deduced on the basis of reasonable assumptions concerning the origin of the observed excess (B–A) differences.

Special Correction for Neutrons

At 3.04 Mev with a hydrogen-filled counter at 8° a neutron background was observed. It was eliminated by changing to an argon filling, the 8° data were repeated, and corrections of -0.52 ± 0.18 percent and -0.66 ± 23 percent were applied, respectively, to the 6° and 7° data.

Gas Contamination Correction

Yields from the 90° contamination counter (Fig. 1) were taken for every data point. Corrections for contaminant gases were only appreciable below 25°, where all scattering cross sections approach Coulomb values. To compute corrections, values are needed for the 90° ratios to Rutherford of the contaminants. The energy dependence of the 90° contaminant yield was well established because of the practice of taking check data at 1.855 Mev. Values for the ratios to Rutherford at 90° were obtained by observing scattering yields as a function of angle from gases which accumulated in the evacuated chamber when hydrogen was not being admitted and by observing the effects of air admitted in the presence of hydrogen. Such data served to determine the ratios to Rutherford within ±30 percent. An uncertainty of this magnitude applies to each correction shown in Fig. 12.

VII. MEASUREMENTS

Proton Energy

The energy of the incident beam was defined by a 90° electrostatic analyzer[7] set for an energy resolution of ±0.1 percent. It was calibrated three times during the scattering work against the $Li^7(p,n)Be^7$ threshold using the value of 1.882 ± 0.002 Mev (abs), as determined by Herb, Snowdon, and Sala.[8] Threshold values were reproducible to ±0.02 percent on the average, which is well within the uncertainty of ±0.1 percent that is quoted for the threshold value.

G Factor

Slit dimensions were measured by means of an improvised traveling microscope employing a ruling engine screw which had been calibrated against a standard meter bar. Observations of the slit-edge positions were reproducible within 0.5 micron, which is consistent with the optical resolution employed. The lengths (h) and (R_0-h) were measured by means of spacer bars which were compared with those distances directly and were then measured with the travelling microscope. Results for the three slit systems are presented in Table I.

Temperatures

Both uniformity and stability of temperatures in the chamber were fairly well insured by the good thermal conductivity and large mass of the aluminum housing which weighed approximately 1200 lb. The bottom of the base plate of the chamber was insulated with polystyrene foam against the heat of the diffusion pumps beneath it and the room temperature was held constant within a few tenths of a degree. Incoming hydrogen was passed through a heat exchanger in contact with the base plate before being admitted to the chamber. Three mercury-glass thermometers graduated in tenths of a degree were placed in oil-filled wells at various points on the base plate and cover plate to measure chamber temperature. They were calibrated at the ice point and at the sodium-sulfate point (32.384°C). The effect of the proton beam upon the temperature of the hydrogen gas was computed and was found to be negligible. An over-all uncertainty of ±0.02 percent has been assigned to the measurements of gas temperature.

Pressure

Hydrogen pressure in the scattering chamber was measured by means of an oil manometer containing Octoil-S diffusion pump oil. The heights of the oil

TABLE I. G-factor dimensions.

Slit system	Width of front slit ($2b_1$) (mm)	Width of rear slit ($2b_2$) (mm)	Length of rear slit (l) (mm)	$G=(4b_1b_2l)/R_0h$ (cm $\times10^6$)
4 mm	3.9932 ± 0.013 percent	3.9893 ± 0.012 percent	20.4593 ± 0.008 percent	$545.580\ \pm0.04$ percent
2 mm	1.9986 ± 0.025 percent	1.9987 ± 0.025 percent	10.1886 ± 0.015 percent	$68.130\ \pm0.08$ percent
1 mm	1.0090 ± 0.050 percent	1.0047 ± 0.050 percent	5.1057 ± 0.030 percent	8.6643 ± 0.14 percent
	$R_0=317.867$ mm±0.006 percent			
	$h=187.934$ mm±0.005 percent			

[7] Warren, Powell, and Herb, Rev. Sci. Instr. **18**, 559 (1947).
[8] Herb, Snowdon, and Sala, Phys. Rev. **75**, 246 (1949).

TABLE II. Systematic uncertainties. The symbol (±) is omitted wherever the sign remains constant for all three slit systems.

Source of error	Uncertainty (percent) 1-mm slits	2-mm slits	4-mm slits	Approximate energy dependence
Energy	0.10	0.10	0.10	Constant in percentage
Proton current	0.10	0.10	0.10	Smooth variation within ±0.1 percent
Capacitance	0.04	0.04	0.04	Constant
Oil density	0.02	0.02	0.02	Constant
Gas contamination	0.30 max	0.33 max	0.3 to 0.0	(See Fig. 12)
Slit edge scattering	0.25 max	0.12 max	0.06 max	Approximately linear in E (see Fig. 13)
G-factor	±0.14 percent	±0.08 percent	±0.04 percent	Constant
Multiple scattering	0.07 max	0.03 max	0.01	E^{-2}

columns were compared to a calibrated precision scale placed between the arms of the U-tube. A precise cathetometer located 1.1 meters from the manometer was used for this purpose. Its accuracy was limited by the optical resolution of its telescopes, and the resulting uncertainty in the height of the oil column was ±0.02 percent. The pycnometer method was used to determine the density and temperature coefficient of the oil and gave for the density in grams per cm³, $d=0.9104+0.00072(25.0°\text{C}-t)$ with an uncertainty of ±0.02 percent.

Current Collection

The proton beam was collected through an aperture 4.2 cm in diameter after traversing a path of approximately 64 cm length in hydrogen at 8-mm Hg pressure. The efficiency of beam collection was determined experimentally by inserting diaphragms of various sizes in front of the collecting aperture, while monitoring the yield of protons at a fixed angle. From the variation of yield with aperture diameter, it was possible to determine an upper limit for the collection loss. The collection loss at 1.85 Mev was concluded to be less than 0.03 percent. This effect should vary as (E^{-2}).

For suppression of secondary electrons, a ring-shaped permanent magnet provided a uniform field of 164 gauss in the space between the window and the cup. This ring was electrically insulated from the housing and was maintained at −900 volts to provide, in addition, an electrostatic barrier. The effectiveness of the electron suppression was determined by varying each suppression field in turn while monitoring the proton yield at a fixed angle. The intensity of suppression field was increased until a saturation of the effect was shown in the measured yield. The uncertainty assigned to electron suppression is ±0.1 percent, which is the statistical uncertainty in the monitoring yield measurements. Pressure in the collector cup housing was maintained at 2×10^{-6} mm Hg.

The condenser in the current integrator was a 4-microfarad polystyrene condenser made by the John E. Fast Company. This condenser had been used by Ralph[9] in 1947 and had been calibrated with ±0.1 percent accuracy by a current-time method. A new calibration with the Maxwell bridge method[10] gave an accuracy of ±0.02 percent for the conditions prevailing in the bridge, i.e., for charging and discharging times of the order of 1/100 sec. The phenomenon of "soak-in" increased the effective capacity by (0.20±0.03) percent for charging cycles of ten seconds and longer. The capacitance measurements, including temperature dependence and soak-in, are considered accurate to ±0.04 percent. The new value of capacitance agrees with the old value given by Ralph within the probable error.

The current integration cycle was the following: The condenser was charged at −10 volts for a period of 30 sec. Collection of proton beam current was then begun simultaneously with the counting of yield. The run continued until the condenser was discharged to zero-volts as indicated by a balanced dc amplifier. At this point, the run was terminated automatically by a relay switch in the output of the dc amplifier. In this operation, the proton current was diverted to ground but the condenser was not shorted. It remained connected to the dc amplifier. Variation in the tripping time of the relay was held to a few hundredths of a percent, and a correction was applied for this error. A means of integrating the grid current from the input tube of the dc amplifier was incorporated in the circuit, enabling that effect also to be made negligible. The uncertainty introduced by the dc amplifier is considered to be ±0.01 percent.

VIII. SUMMARY OF UNCERTAINTIES

The uncertainties in the various corrections are divided into two categories according to their effect

TABLE III. Nonsystematic uncertainties.

Source	Representative value of uncertainty (percent)	Remarks
Statistics	±0.22	$100\,N^{-\frac{1}{2}}$
Height of oil column	±0.02	Limited by optics
Gas temperature	±0.02	
Counting losses	±0.02	Reaches ±0.15 at 60°
Counter performance	negligible	Reaches ±0.04
X-ray electrons	negligible	Reaches ±0.2 percent at 7 points
Resolution (geometrical)	negligible	
Beam size	negligible	

[9] D. C. Ralph, Ph.D. thesis, University of Wisconsin (1949) (unpublished).

[10] H. L. Curtis, *Electrical Measurements* (McGraw-Hill Book Company, Inc., New York, 1937).

upon the interpretation of the data. An error is regarded as "systematic" if it is constant with angle or if its angular dependence appreciably resembles that of a P wave or D wave anomaly. Values of systematic uncertainties are listed in Table II.

The "nonsystematic" uncertainties are listed in Table III. The second and third items, as well as the first, are considered statistical, since they were measured in each individual run and accuracy was limited by the sensitivity of the measuring devices. These three uncertainties are added quadratically. That resultant is then added linearly to the sum of all other nonsystematic uncertainties, including the uncertainties in special corrections not listed here. The total is tabulated with each value of the cross section in Table IV.

IX. EXPERIMENTAL PROCEDURE

Angular Distributions

Angular distribution runs were usually preceded by a preliminary survey of counting conditions and of operating conditions in general. Then, before the regular measurements were begun, standardization measurements were made at 1.855 Mev. The absolute cross section was measured at two points at that energy as a check on the reproducibility of results. After these so-called "check points" had been measured, the regular measurements were begun.

Angular distribution measurements were usually made in the direction of increasing angle. Generally the 1-mm slits were used from 6° to 10°, the 2-mm slits from 10° to 15°, and the 4-mm slits from 15° upward. Whenever conditions permitted, the measurements were extended beyond 45° in order to check the symmetry of the cross section about 90° in the center-of-mass, but no special efforts were made to obtain such data at all energies. At each angle, a total of approximately 200 000 counts was accumulated. These were equally distributed between the measurements at the left and the right of the incident beam. Individual runs corresponded to the collection of 40 micro-coulombs of incident charge and varied in number between two and ten according to the magnitude of the yield. Care was taken to vary the sequence of left- and right-hand measurements so that

TABLE IV. Experimental values of the differential cross section in the center-of-mass system.

	1.858 Mev[a] (July 10)		1.855 Mev (June 18)		2.425 Mev (June 20, 23)		3.037 Mev (June 26)	
θ c.m.	$\sigma_{c.m.}$ (barns)	P.E.[b] percent	$\sigma_{c.m.}$ (barns)	P.E. percent	$\sigma_{c.m.}$ (barns)	P.E. percent	$\sigma_{c.m.}$ (barns)	P.E. percent
12°	...	...	...	...	6.41529	±0.26	4.04698	±0.30
14°	5.75321	±0.27	5.76721	±0.26	3.33742	±0.32	2.10501	±0.33
16°	3.25245	±0.29	3.26649	±0.31	1.89917	±0.34	1.21101	±0.40
20°	1.25760	±0.21	1.26017	±0.19	0.75311	±0.22	0.49519	±0.30
24°	0.59277	±0.25	0.59828	±0.29	0.37787	±0.29	0.26680	±0.35
30°	0.27824	±0.21	0.27778	±0.17	0.20453	±0.15	0.16286	±0.49
35°	0.19750	±0.26	0.19675	±0.15[c]	0.16273	±0.22	0.13868	±0.29
40°	0.16763	±0.20	0.16732	±0.21	0.14922	±0.28	0.13160	±0.20
50°	0.15594	±0.23	0.15590	±0.17	0.14673	±0.26	0.13203	±0.25
60°	0.15992	±0.21	0.15958	±0.12	0.15064	±0.23	0.13615	±0.26
70°	0.16420	±0.25	0.16416	±0.22	0.15467	±0.21	0.13832	±0.28
80°	0.16753	±0.24	0.16737	±0.46	0.15708	±0.20	0.14067	±0.23
90°	0.16793	±0.28	0.16775	±0.30	0.15686	±0.24	0.14084	±0.28
100°	...	...	...	...	0.15604	±0.28	0.14060	±0.33
110°	...	...	...	...	0.15450	±0.37	0.13953	±0.39
120°	...	...	...	...	0.15012	±0.49	0.13579	±0.54

	3.527 Mev (June 30)		3.899 Mev (July 2)		4.203 Mev (July 5)	
θ c.m.	$\sigma_{c.m.}$ (barns)	P.E. percent	$\sigma_{c.m.}$ (barns)	P.E. percent	$\sigma_{c.m.}$ (barns)	P.E. percent
12°	2.99318	±0.28	2.44610	±0.47	2.10983	±0.48
14°	1.57734	±0.33	1.28660	±0.60	1.10775	±0.82
16°	0.90700	±0.46	0.74649	±0.34	0.64336	±1.11
20°	0.38055	±0.28	0.32162	±0.35	...	...
25°	0.19410	±0.45	0.17095	±0.56	0.15415	±0.45
30°	0.14090	±0.21	0.12769	±0.27	0.11882	±0.32
35°	0.12442	±0.25	0.11479	±0.35	0.10825	±0.35
40°	0.12056	±0.20	0.11252	±0.19	0.10652	±0.30
50°	0.12139	±0.21	0.11379	±0.31	0.10815	±0.32
60°	0.12526	±0.25	0.11705	±0.33	0.11104	±0.33
70°	0.12769	±0.26	0.11900	±0.36	0.11316	±0.29
80°	0.12925	±0.24	0.12027	±0.29	0.11403	±0.29
90°	0.12926	±0.28	0.12062	±0.26	0.11420	±0.31
100°	0.12885	±0.28	0.12074	±0.25	0.11400	±0.34
110°	0.12754	±0.45	0.11924	±0.36	...	...
120°	...	...	0.11674	±0.53	...	...

[a] Low pressure run, H_2 at 6.12-cm oil. Pressure in other runs was 11.4-cm oil.
[b] Only the "nonstematic" uncertainties are listed here (see Sec. VII).
[c] This point obtained on June 23.

TABLE V. Cross sections at 1.855-Mev check points. Cross sections are given in barns per steradian in center-of-mass system. Angles are in the laboratory system. In general the number of counts taken at check points was 600 000 at 15°, 350 000 at 17.5°, and 300 000 at 30°.

Date	(15°)	(17.5°)	(30°)
June 18	0.27840		0.15973
	0.27771		0.15943
	0.27786		
June 20	0.27899		0.16008
June 23	0.27876	0.19675	0.15987
June 25	0.27873		0.15946
			0.16011
June 27	0.27869		0.15965
June 30	0.27900		0.15973
July 1	0.27861	0.19722	0.16048
July 2		0.19649	0.15986
July 4		0.19643	0.16046
July 5		0.19656	0.16021
July 10[a]		0.19745	0.15992
Wtd. average	0.27824	0.19673	0.15992
Rms deviation	0.16 percent	0.15 percent	0.21 percent

[a] These points were taken at 1.858 Mev. They have been adjusted to 1.855 Mev for presentation here but are not included in the average.

an asymmetry could be distinguished from a time-dependent variation. At the conclusion of most runs, a check was made upon the constancy of the experimental conditions by repeating some measurement made earlier in the run. Occasionally the cross sections at 1.855 Mev were remeasured also.

Check Points

The cross sections at 15° and 30°, 1.855 Mev, were used for standardization of the measurements. These so-called "check points" served to establish the reproducibility of measurements, to monitor the over-all performance, and to separate the effects of certain of the variables. The 30° point served to check the absolute accuracy of the apparatus, since it is relatively insensitive to energy and angle and is practically free of influence from the spurious effects appearing at low angles. Changes affecting the pressure, temperature, current integration, or G factor are revealed there. The 15° point, on the other hand, had nearly the maximum sensitivity to spurious low angle effects such as gas-contamination, and it is highly sensitive to the energy. An error of 0.1 percent in energy causes an error of almost 0.2 percent in the 15° cross section. The 15° point had the disadvantage of a very high counting rate. Too frequently reduction of the beam current was required in order to meet the restrictions on counting rate. For that reason the 17.5°, 1.855-Mev point was chosen to replace the 15° point later in the experiment. The check point data are summarized in Table V.

X. RESULTS

Final values of the differential scattering cross section obtained in this experiment are listed in Table I. The uncertainties listed with the values of the cross section are the "nonsystematic" uncertainties which may affect the cross section irregularly from point to point. In Fig. 10, the data for the central range of angles are plotted together with the 1939 Wisconsin data[11] and the 1948 Minnesota data.[12] Agreement is satisfactory. The data are fitted with theoretical curves for a pure S-wave anomaly in the range from 25° to 45°, and, at each energy, the S wave is seen to account adequately for the cross sections. At low angles, however, there are definite departures from the pure S wave at all energies. These deviations are shown in Fig. 11 where the percentage deviation from the theoretical S-wave cross section is plotted as a function of angle. Arbitrary curves have been drawn through the data to indicate the general trend of the low angle anomaly with energy and angle. It should be noted that the 4.2-Mev data below 25° (12.5° lab angle) are of poor quality. The 20° point is missing entirely because the 2-mm slits were accidentally set in the wrong position. The points below 20° are of little weight because of the

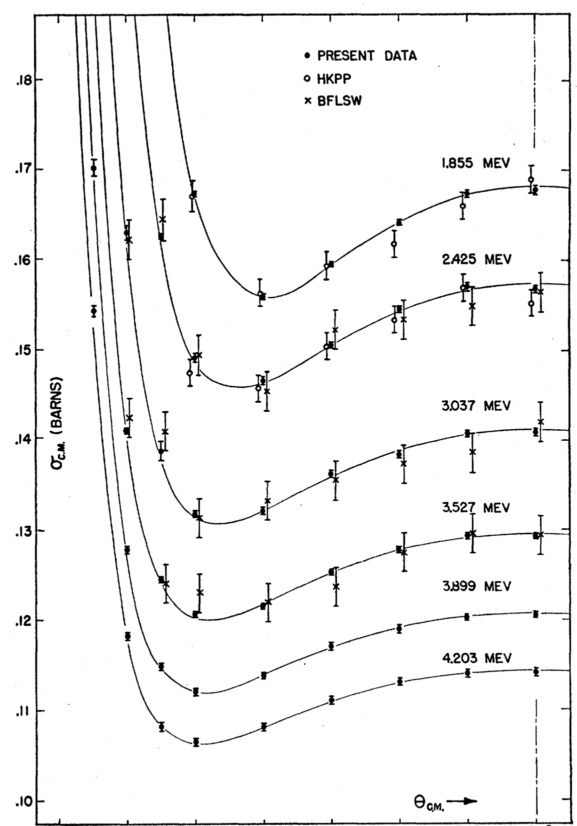

FIG. 10. A comparison of the present results with those of Herb, Kerst, Parkinson, and Plain (HKPP) and those of Blair, Freier, Lampi, Sleator, and Williams (BFLSW). The curves are calculated to fit the present data assuming a pure S-wave anomaly. Only the nonsystematic errors are shown by the uncertainty bars since only that class of uncertainties may be used to account for random deviations from the smooth curves.

[11] Herb, Kerst, Parkinson, and Plain, Phys. Rev. **53**, 239 (1938).

[12] Blair, Freier, Lampi, Sleator, and Williams, Phys. Rev. **74**, 553 (1948).

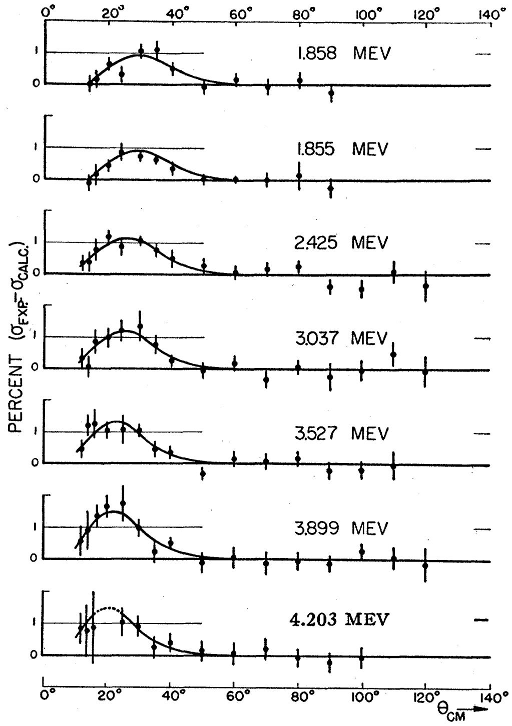

FIG. 11. Observed departures from cross sections calculated to fit the data assuming a pure S-wave anomaly. Uncertainty bars represent the nonsystematic uncertainties.

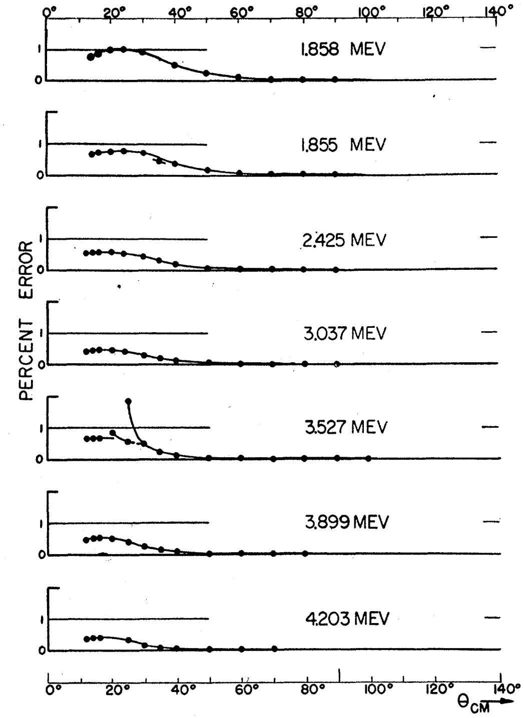

FIG. 12. Percentage contribution from gas contamination. Applied corrections are negative and have an uncertainty of ± 30 percent. Discontinuities in curve for 3.5 Mev resulted from momentary air leaks in slit-changing mechanism.

large uncertainties introduced by the slit penetration effect noted earlier.

The conspicuous feature of these low angle deviations is that they do have the general form of a repulsive P-wave anomaly, especially at the lower energies. The definite maximum between 20° and 30°, center-of-mass angle, and the sharp decline at lower angles are strong indications that the anomaly is of nuclear origin. No single systematic error has such a form. It is conceivable that a combination of errors might produce deviations of this form, but no admissible variation in the magnitudes of the applied corrections will remove the anomalies shown here. This can be seen in part from Figs. 12 and 13, in which the larger errors of the experiment are plotted on the same scale as the data of Fig. 11. These are actually plots of the applied corrections, but the ordinates are reversed in sign so that the errors which have been removed from the data may be compared directly with the anomalies which remain. Apart from the behavior at very low angles, both the gas-contamination error and slit-edge scattering error have somewhat the form of the low angle anomaly, and that is true also for errors due to energy, beam current, and G factor, which introduce the only other appreciable systematic uncertainties. Taking the linear sum of the uncertainties in all of these quantities, together with the linear sum of nonsystematic uncertainties, one should obtain a fairly generous estimate of the limit

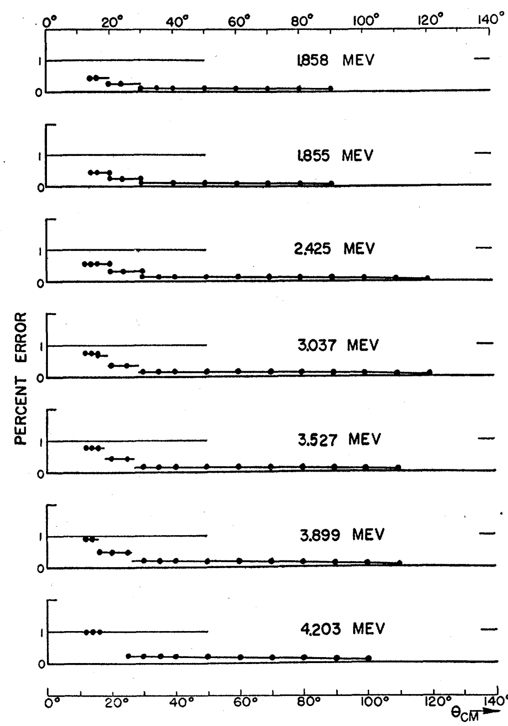

FIG. 13. Percentage contribution from slit-edge scattering. Applied corrections are negative and have an uncertainty of ± 25 percent.

of error in the data. The anomalies in Fig. 11 lie outside of such limits of error. Since the uncertainties are largely based upon experimental evidence and are considered to be reasonably conservative, the fact that the anomalies are larger than the uncertainties is considered significant. Even if one were to suspect the accuracy of the uncertainty, estimates and were to speculate upon the effect of increasing the sizes of certain corrections, it would still be necessary to observe some restrictions as to the energy dependence of the errors. When that is done it is found difficult to eliminate the anomaly at one energy without causing a considerable deviation at some other energy. Thus, there appears to be little possibility that the low angle anomaly is due to any of the known sources of error. If unknown and unsuspected errors are the cause of the anomalies, it is almost certainly necessary that two different errors be present in order to cause deviations of the form observed. That possibility seems unlikely but it obviously cannot be excluded except by repetition of the experiment under a variety of conditions and by different persons.

A theoretical analysis of these data has been made by J. L. Powell and H. H. Hall and is presented in the accompanying paper. For a central potential they find that a negative P-wave phase shift fits the data at each energy reasonably well within the limits of uncertainty. The phase shift varies fairly regularly from $K_1=-0.05°$ at 1.855 Mev to $K_1=-0.11°$ at 3.9 Mev. At 4.2 Mev however, the value falls to $K_1=-0.07°$. It is not surprising that the 4.2-Mev value should be irregular, considering the poor quality of the data there, but it is surprising that the uncertainties do not readily admit a continuation of the trend of the lower energy data. The effect may be real, but it seems more likely that the determination of K_1 at 4.2 Mev depends too strongly upon one or two data points and is, therefore, much more susceptible to error than are the values at other energies. If any use is made of the 4.2-Mev low angle data, it should be done only with complete and cautious regard for the uncertainties in those data.

The authors desire to express their appreciation to R. G. Herb for his guidance in this work. They are indebted also to D. C. Ralph, who originally proposed the large scattering chamber and gave much valuable help on design problems. They wish to thank H. A. Krueger, who performed the difficult task of condenser calibration, and the members of the departmental shop, who contributed to the design as well as the construction of the apparatus. Many other members of the department deserve sincere thanks for their valuable assistance.

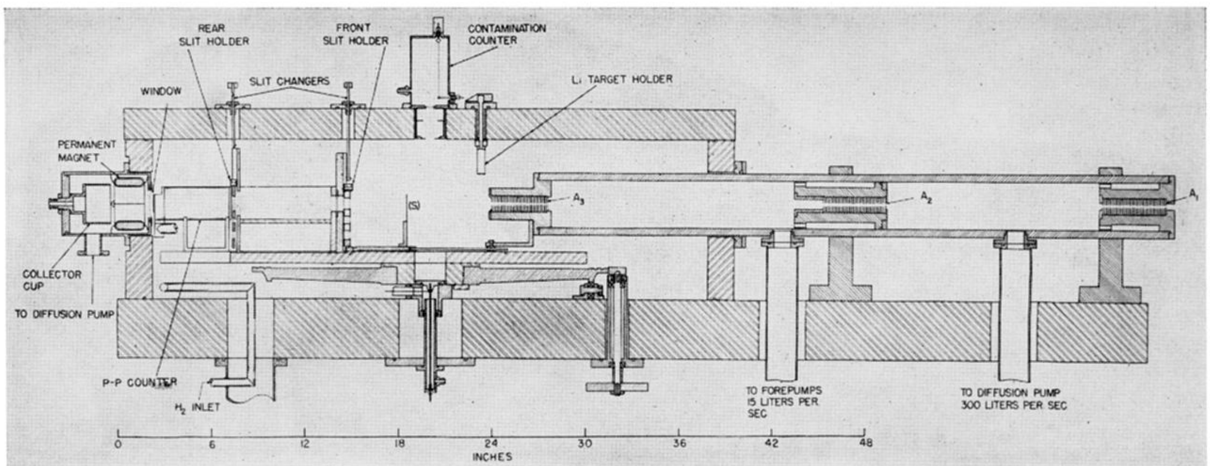

FIG. 1. Vertical cross section of chamber with analyzer slit assembly at zero-angle.